PAPER

Multi-responsive hybrid particles: thermo-, pH-, photo-, and magneto-responsive magnetic hydrogel cores with gold nanorod optical triggers†

Supparesk Rittikulsittichai,[a] Arati G. Kolhatkar,[a] Subhasis Sarangi,[b] Maria A. Vorontsova,[c] Peter G. Vekilov,[c] Audrius Brazdeikis[b] and T. Randall Lee*[a]

The research strategy described in this manuscript harnesses the attractive properties of hydrogels, gold nanorods (Au$_{rods}$), and magnetic nanoparticles (MNPs) by synthesizing one unique multi-responsive nanostructure. This novel hybrid structure consists of silica-coated magnetic particles encapsulated within a thermo-responsive P(NIPAM-*co*-AA) hydrogel network on which Au$_{rods}$ are assembled. Furthermore, this research demonstrates that these composite particles respond to several forms of external stimuli (temperature, pH, light, and/or applied magnetic field) owing to their specific architecture. Exposure of the hybrid particles to external stimuli led to a systematic and reversible variation in the hydrodynamic diameter (swelling–deswelling) and thus in the optical properties of the hybrid particles (red-shifting of the plasmon band). Such stimuli-responsive volume changes can be effectively exploited in drug-delivery applications.

Introduction

Research involving hybrid particles has received considerable attention due to their versatility in emerging applications. Some of the most useful hybrid particles combine disparate components into one single nanostructure, where each component possesses a characteristic shape/structure and functionality. Most interestingly, hybrid particles can be designed to possess numerous features that enable several tasks to be performed simultaneously. Among the different classes of materials, hydrogel particles utilizing copolymers that include *N*-isopropylacrylamide (NIPAM) monomers have been widely employed as templates for constructing hybrid particles[1,2] because of the thermoresponsive properties of these polymers; they exhibit a dramatic change in volume at a tunable transition temperature.[3–6] Introducing acrylic acid (AA) monomer into the PNIPAM chain (forming P(NIPAM-*co*-AA)) increases the LCST (lower critical solution temperature; the temperature where swelling/collapsing occurs) of the copolymer from 32 °C

to as high as 60 °C, depending upon the amount of added AA. This modification to PNIPAM allows heating over a larger temperature range using, for example, magnetic nanoparticles (MNPs) in the core of a hydrogel/MNP hybrid nanostructure, where the activating heat is generated by exposing the MNPs to an oscillating magnetic field.[7] Additionally, under basic conditions, the P(NIPAM-*co*-AA) hydrogel structure expands due to the electronic repulsion of the carboxylate groups within the hydrogel network, while under certain acidic conditions, the network collapses due to the loss of electronic repulsions.[8] Owing to these advantageous properties, P(NIPAM-*co*-AA) hydrogels have been embedded with MNPs and/or optical nanomaterials for applications in controlled drug delivery.[1,9–15,16] Due to the intrinsic flexible structure of the hydrogels, (1) metallic nanoparticles can be dispersed or assembled within the polymer network[17–25] and (2) drugs, enzymes, and other active biomolecules can be bound and/or entrapped within the polymer network and controllably released from the interior.[26–28] Such releases are also facilitated by the large volume transitions that occur during the swelling–collapsing of the networks initiated by external stimuli (*e.g.*, temperature, pH, or ionic strength),[7,8,29–34] thus rendering them attractive candidates for use not only in drug delivery,[26–28] but also in catalysis[35,36] and photonic applications.[36]

To couple these useful properties, several researchers have developed hybrid particles comprised of inorganic nanoparticles and hydrogels, either (i) as core–shell

[a]Department of Chemistry and the Texas Center for Superconductivity, University of Houston, 4800 Calhoun Road, Houston, TX 77204-5003, USA. E-mail: trlee@uh.edu
[b]Department of Physics and the Texas Center for Superconductivity, University of Houston, 4800 Calhoun Road, Houston, TX 77204-5003, USA
[c]Department of Chemical and Biomolecular Engineering, University of Houston, 4800 Calhoun Road, Houston, TX 77204-5003, USA

structures[10,37–39] or (ii) as randomly distributed nanoparticles within the hydrogel network.[17–25] To provide background for our results, two specific examples are outlined below.

(i) *Core–shell structures*. This hybrid system utilizes a hydrogel polymer network and MNPs having core–shell structures,[10,37,40,41] where the MNPs are encapsulated within the hydrogel network. The hydrogel component acts as a drug container and transducer simultaneously. For this system, the magnetic components are anticipated to function as energy transformers by converting energy received from an oscillating magnetic field into heat. Increased temperatures induce volumetric changes in the hydrogel component.[40]

(ii) *Nanoparticles distributed within the hydrogel*. This hybrid system consists of hydrogels loaded with gold nanorods (Au$_{rods}$), which can be designed to absorb in the near infrared (NIR) spectral region.[18–20,22,25] Here, the volume transitions of the hydrogel component are driven by irradiation with NIR lasers. The Au$_{rods}$ serve as antennae, absorbing NIR light that is converted into heat energy, affording an increase in temperature for the irradiated areas.

As a consequence of the change in temperature in both of these hybrid systems, the hydrogel structure collapses and expels its liquid contents from the interior network. Based on these mechanisms, the hybrid hydrogel system can potentially be used in controlled-release drug applications, where a drug can be loaded/entrapped, guided to a specific location, and subsequently released upon introduction of an oscillating magnetic field or NIR laser irradiation, thereby enabling magneto-photothermal drug delivery. Several examples of magnetic thermal-responsive microspheres are known.[9–12,42–47] Nevertheless, the reported hybrid particles typically contain small magnetic cores, which give poor dynamic responses to magnetic stimuli (<1 emu g^{-1}),[11,44] poor manipulation by an external magnetic force, and insufficient heat generation when being subjected to an oscillating magnetic field. More impor-

tantly, problems encountered with irregular core/shell structures or polydisperse size distributions[11,12,42,43] can adversely affect their pharmacological properties. More recently, there has been research on supramolecular hydrogels that respond to external stimuli;[48] however, due to their complicated syntheses, their applications are limited.

In the work presented here, we report the synthesis and characterization of hybrid particles consisting of a relatively large magnetic core, which is consecutively encapsulated by silica and P(NIPAM-*co*-AA) hydrogel shells, and then subsequently covered with gold nanorods (see Scheme 1). PNIPAM-coated iron oxide (Fe$_3$O$_4$) particles have been previously reported by Wang *et al.*,[49] but the addition of AA units in the PNIPAM hydrogel network also renders our hybrid particles responsive to pH stimuli. In addition to tracking the photothermal volume change triggered by the Au$_{rods}$ upon near IR exposure, we evaluated the effect of changes in pH and the presence of an oscillating magnetic field. Harnessing these unique properties of hydrogels, Au$_{rods}$, and MNPs by creating one multi-responsive nanostructure served as the motivation for our work described here. Furthermore, we demonstrated that the response of our composite particles to external stimuli (pH, temperature, light, and/or applied magnetic field) is a function of its composition and architecture. Such multi-functional hybrid particles should satisfy the technological requirements for discreet particle-based drug delivery vehicles.

Experimental section

Materials

The following chemicals were obtained from the indicated suppliers and used as received: sodium acetate anhydrous (Mallinckrodt Baker), iron(III) chloride hexahydrate (FeCl$_3$·6H$_2$O, Alfa Aesar), cetyltrimethylammonium bromide
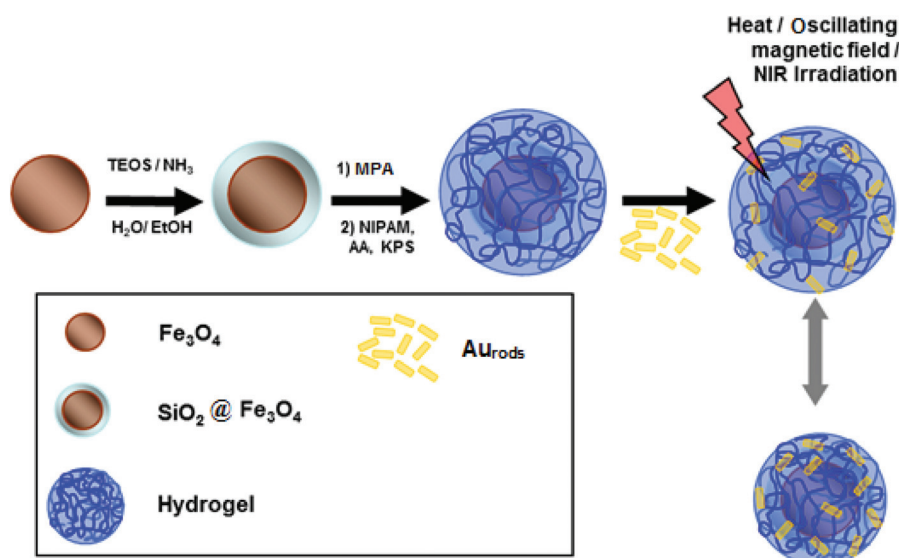
Scheme 1 Strategy used to prepare multi-responsive hydrogel particles.

(CTAB, high purity grade, Amresco), and tetrachloroauric(III) acid hydrate, ($HAuCl_4 \cdot 3H_2O$, Strem). Ammonium hydroxide (with 30% NH_3 content), ethylene glycol (EG), and ethanol were obtained from EM Science. For polymerizations, N-iso-propylacrylamide (NIPAM, 99.0%), acrylic acid (AA, 99.0%), N,N'-methylenebisacrylamide (BIS, 96.0%), 3-(trimethoxysilyl) propyl methacrylate (MPA, 98.0%) were purchased from Acros. Sodium sulfide nonahydrate ($Na_2S \cdot 9H_2O$), sodium borohydride ($NaBH_4$), potassium persulfate (KPS, 99.0%), and tetraethyl-orthosilicate (TEOS, 98.0%) were obtained from Aldrich. The water used for all reactions was purified to a resistivity of 18 MΩ cm and filtered through a 0.22 μm filter membrane to remove any impurities (Academic Milli-Q Water System; Millipore Corporation). All glassware and equipment were cleaned using aqua regia solution and rinsed with Milli-Q water prior to use.

Synthesis of multi-responsive MNPs

The synthesis of the targeted hybrid MNPs was achieved by first preparing hydrogel-encapsulated-silica-coated Fe_3O_4 MNPs and Au_{rods} separately, and then assembling the Au_{rods} on the outermost hydrogel surface.

Synthesis of Fe_3O_4 MNPs. The targeted magnetic Fe_3O_4 particles were synthesized by modification of a procedure reported by Li and co-workers,[50] which is described in the ESI.†

Synthesis of SiO_2 Shell@Fe_3O_4 Core (SiO_2@Fe_3O_4). The surfaces of the magnetic particles were coated with uniform silica shells using a modification of a procedure reported by Stöber *et al.*[51] which is provided in the ESI.†

Hydrogel coating of SiO_2@Fe_3O_4 (hydrogel@SiO_2@Fe_3O_4). To effect hydrogel encapsulation, the surfaces of the SiO_2@Fe_3O_4 MNPs were functionalized with vinyl groups. The suspension of 1.3×10^{15} MNPs per mL SiO_2@Fe_3O_4 (20.0 mL) was mixed with MPA (0.20 mL) under vigorous stirring. The reaction mixture was stirred for 24 h at rt; the temperature was then elevated to 85 °C to improve the bond affinity between MPA and the silica shell. The resultant particles were magnetically separated and washed with ethanol several times before redispersing in 5.0 mL of ethanol. The hydrogel-shell structure was formed through a free radical co-precipitation polymerization. An aqueous solution containing NIPAM, AA, and BIS was mixed with MPA-modified SiO_2@Fe_3O_4 ethanol solution (2.5 mL). The solution was mechanically stirred at 400 rpm and degassed with argon for 15 min. The solution was then heated to 70 °C under a blanket of argon, which was followed by the addition of KPS (0.02 g mL^{-1}) to initiate the polymerization. The coated nanoparticles were washed with deionized water and removed from unattached hydrogel particles by magnetic separation and then redispersed in 10.0 mL of water. Notably, the thickness of the hydrogel can be systematically varied by adjusting the amount of monomer, cross-linker, and initiator.[2,5,52,53]

Preparation of gold nanorods (Au_{rods}). The Au_{rods} were prepared using the protocol developed by Nikoobakht,[54] which is described in the ESI.†

Assembly of Au_{rods} on the hydrogel@SiO_2@Fe_3O_4 particles.[18,25] To assemble the Au_{rod} particles on the surface of the hydrogel, a dispersion of Au_{rods} and hydrogel@SiO_2@Fe_3O_4 particles were mixed at a volume ratio of 5 : 1, respectively, under continuous sonication for 30 min. To remove any unattached Au_{rod} particles, the resulting Au_{rods}-hybrid MNPs were twice centrifuged and re-suspended in water.

Characterization of the hybrid particles

The composite particles were characterized using a variety of instrumental methods to provide data regarding their size and morphology, magnetic properties, light absorption and scattering properties, and composition.

SEM/TEM imaging. SEM imaging was used to characterize the average size and size distribution of the Fe_3O_4 MNPs. The morphology of the hybrid particles was also evaluated using a LEO-1525 scanning electron microscope (SEM) operating at 15 kV. To obtain high-resolution SEM images, all samples were deposited on a silicon wafer for analysis. Similarly, the particle size and morphology were also evaluated by employing a JEM-2000 FX transmission electron microscope (TEM) operating at an accelerating voltage of 200 kV. All TEM samples were deposited on 300 mesh holey carbon-coated copper grids and dried overnight before analysis.

Hydrodynamic diameter. The hydrodynamic diameter of the hydrogel@SiO_2@Fe_3O_4 particles was measured as a function of temperature and pH using two different methods (i) dynamic light scattering and (ii) recorded magnetic relaxation. (i) Dynamic light scattering. The DLS data were collected by an ALV light scattering device equipped with a He–Ne laser (λ = 632.8 nm, 35 mW) and an ALV-5000/EPP Multiple τ Digital Correlator. The autocorrelation functions were acquired at 90° for 60 s. For each sample, we collected 10 autocorrelation functions. To allow convection to dampen, data collections started 20 min after the solution was introduced to the cuvette. From the autocorrelation functions, we determined the average values of the particle diameter and the confidence interval of the determination. (ii) Recorded Magnetic Relaxation (MRX).

Brownian relaxations of hybrid particles were studied at room temperature using a custom-built superconducting quantum interference device (SQUID) system by measuring the decay of the magnetic field immediately after removing the magnetizing field.[43] The system was equipped with a 12 mm superconducting pick-up coil configured as a first-order gradiometer with a 50 mm baseline and was controlled by dc-SQUID electronics. Hybrid magnetic particle suspensions placed under the SQUID sensor were exposed to a magnetizing field of 3 mT for 1 s before recording the signal decay by computer. The recorded magnetic relaxation curves were analyzed, and the hydrodynamic diameters of the hydrogel@SiO_2@Fe_3O_4 particles were calculated as a function of temperature and pH.

X-ray photoelectron spectroscopy (XPS). XPS analysis was carried out using a PHI 5700 XPS instrument equipped with a monochromatic Al Kα X-ray source ($h\nu$ = 1486.7 eV) incident at 90° relative to the axis of a hemispherical energy analyzer. The

spectrometer was operated at high resolution with a pass energy of 23.5 eV. The photoelectron takeoff angle was 45° from the sample surface, and the analyzer spot diameter was set to 2 mm. The binding energies for the collected spectral data were referenced by setting the $Au_{4f7/2}$ binding energy to 84.0 eV.

Magnetic properties. The magnetic properties of the samples were evaluated using a vibrating sample magnetometer (VSM, LakeShore VSM 7300 Series with LakeShore 735 Controller and LakeShore 450 Gaussmeter Software Version 3.8.0) at rt. Data were collected for the Fe_3O_4 core, $SiO_2@Fe_3O_4$, and hydrogel@$SiO_2@Fe_3O_4$ particles.

Light absorption measurements. All UV visible spectra were recorded using a Cary 50 Scan UV-visible spectrometer. In addition to analysis of their light absorption/scattering properties in the UV-visible range, the hydrogel hybrid particles (3.0 mL) were loaded in a quartz cuvette and irradiated by a diode laser (AixiZ, CW 300 mW, 808 ± 10 nm) at a power density of ~5 W cm^{-2} for 5 min. During the course of irradiation, the temperature of the suspension was measured every 1 s using a fiber optic GaAs temperature sensor (Neoptix, T1) with a temperature resolution of ±0.1 °C. After exposure, the spectrum of the hybrid particles was measured instantaneously (within 30 s).

Magnetic field heat generation. To evaluate the heat-generating capacity of the hybrid particles, a 1.2 kW custom-made electromagnetic field generator was built around an N-channel power MOSFET (Metal Oxide Semiconductor Field Effect Transistor) using a DC power supply (Xantrex, XRF) and a function generator (Agilent, 33120A) to produce an alternating magnetic field having an amplitude of 0–10 kA m^{-1} at a frequency of 60–215 kHz. The field coil (11 turns, OD 12 mm, L 50 mm) was constructed from a copper tubing (OD 3.2 mm) and tuned to

100 kHz using a matching network. The field coil was cooled with a closed-loop, circulating water system stabilized at 30 °C by a solid-state thermoelectric water chiller (ThermoTek, T251P-2). In addition, a high-density foam insert was used to secure the sample and to reduce direct heat conduction from the coil to the sample. The temperature of the sample solution was measured every 1 s using a fiber optic GaAs sensor (Neoptix, T1) with a resolution of ±0.1 °C.

Results and discussion

Morphology of hybrid particles

The synthesis of the hybrid particles consisting of $Au_{rods}@$ hydrogel@$SiO_2@Fe_3O_4$ was conducted in three stages as illustrated in Scheme 1. The first stage started with the synthesis of Fe_3O_4 magnetic particles with an average particle diameter of ~115 nm (see Fig. S1 in the ESI†), followed with the growth and deposition of SiO_2 onto the magnetic particles using a modification of a procedure reported by Stöber et al.[55] The silica layers were directly deposited onto the magnetic microspheres without any surface modification due to the strong affinity of Fe_3O_4 toward silica precursors via their hydroxyl groups.[56–58] SEM and TEM images of the Fe_3O_4 particles encapsulated by ~50 nm silica shells are provided in Fig. 1a and e, respectively.

The second stage involved the functionalization of the surface of the silica shell with MPA to afford pendant vinyl groups attached to the surface of silica. The resulting MPA-modified magnetic $SiO_2@Fe_3O_4$ particles were used as templates from which NIPAM and AA monomers were copolymerized by using BIS as a crosslinker and KPS as an initiator, thus leading to the formation of a P(NIPAM-co-AA) layer around the
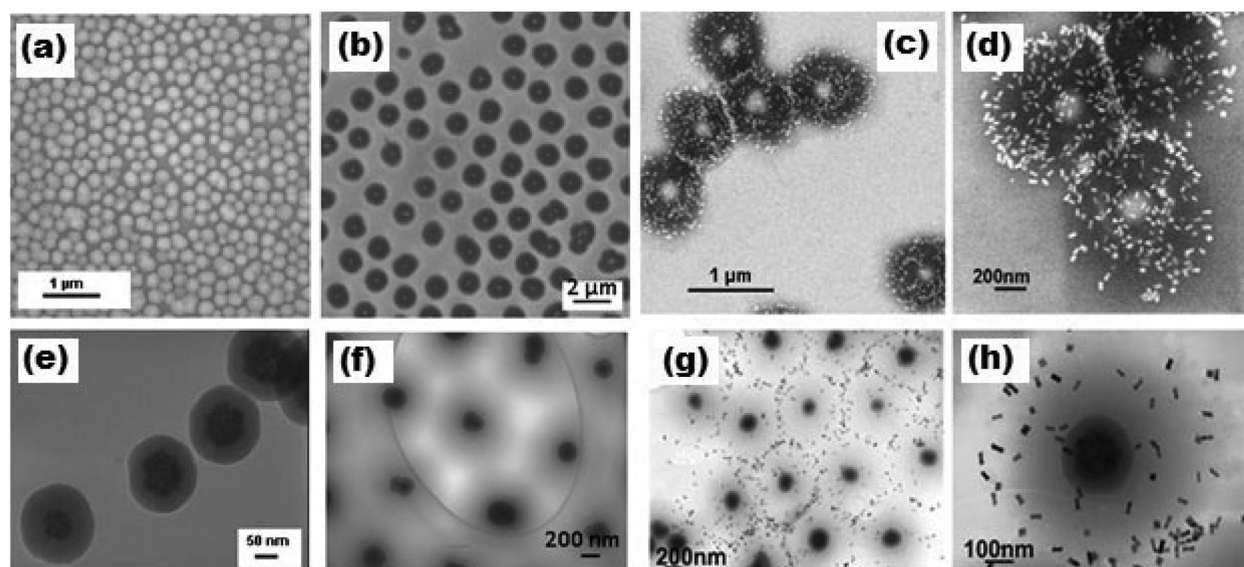

Fig. 1   Top row: SEM images of (a) $SiO_2@Fe_3O_4$ MNPs and (b) hydrogel@$SiO_2@Fe_3O_4$ MNPs, along with $Au_{rods}@$hydrogel@$SiO_2@Fe_3O_4$ hybrid MNPs at (c) low magnification and (d) higher magnification. Bottom row: (e–h) respective TEM images of a–d.

$SiO_2@Fe_3O_4$ cores. Notably, the introduction of AA units into the hydrogel network not only promotes the sensitivity to pH, but also provides a negatively charged hydrogel surface at a pH above its pK_a of 4.2.[5,8,18,22,25]

Fig. 1b and f provide SEM and TEM images for the $SiO_2@Fe_3O_4$ core encapsulated by a hydrogel shell (hydrogel@$SiO_2@Fe_3O_4$) having a total diameter of ~1.2 µm. The SEM image reveals the core/shell structure, and the TEM image provides additional detail for the core/shell architecture due to their differences in electron densities. The dark centers are ascribed to the Fe_3O_4 cores consecutively encapsulated in a gray silica interlayer and then a white-gray hydrogel outer layer. Additionally, the TEM images allow an estimation of the thickness of the hydrogel shells (~500 nm). Nevertheless, the SEM and TEM images reflect the particle sizes in a dried state; therefore, we used DLS and MRX to evaluate the size of the hybrid particles in swollen states under various temperature and pH conditions. The overall diameters of the composite hydrogel@$SiO_2@Fe_3O_4$ hybrid particles obtained from measurements by SEM, TEM, DLS, and MRX are summarized in Table 1.

In the final stage, the negatively charged hydrogel layer was treated with a solution containing positively charged Au_{rod} particles;[18,25,59] the resulting attractive electrostatic interaction led to the formation of gold-decorated hybrid particles.[18-20,22,25] We used FE-SEM and TEM to evaluate the morphology of the hybrid particles. The SEM images in Fig. 1c and d show that $SiO_2@Fe_3O_4$ particles (bright cores) were encapsulated within the hydrogel layer (dark shells), and the Au_{rod} particles (bright

rods) were dispersed across the hydrogel layer. The TEM images in Fig. 1g and h further illustrate the structure of the hybrid particles, in which each component can be discerned due to the differences in electron density. The dark spots correspond to Fe_3O_4 particles that are coated with an overlayer of silica (dark gray color), which is further coated with a thick layer of hydrogel (light gray color) that has Au_{rod} particles (black rods) attached on the surface. The SEM and TEM images allow an estimation of the overall diameter of the hybrid particles (~1 µm).

Surface composition

We employed XPS to characterize the hydrogel layer-encapsulated $SiO_2@Fe_3O_4$ cores. The existence of the hydrogel was verified by the presence and position of C 1s, N 1s, and O 1s peaks (Fig. 2a) at ~284, 400, and 531 eV, respectively. In addition, the C 1s curve was fitted (Fig. 2b) with three different peak components assigned as (1) hydrocarbon moieties (C_xH_y: 284.5 eV), (2) carbons adjacent to carbonyl groups or proton-bearing carbons attached to nitrogen (C–C=O and C–N: 285.7 eV), and (3) carbonyl carbons (C=O: 287.4 eV).[60,61] These XPS data provide strong evidence that P(NIPAM-co-AA) was grafted onto the $SiO_2@Fe_3O_4$ surface.

Magnetic properties

VSM was used to obtain the magnetization curves of the samples. The saturation magnetization of two distinct samples of hydrogel@$SiO_2@Fe_3O_4$ particles were 4 and 3 emu g^{-1}, respectively (Fig. 3). The decrease in saturation magnetization,

Table 1 The reactants used and the resulting composite particle diameters obtained as determined by SEM, TEM, DLS, and MRX measurements at 25 °C for two particle samples

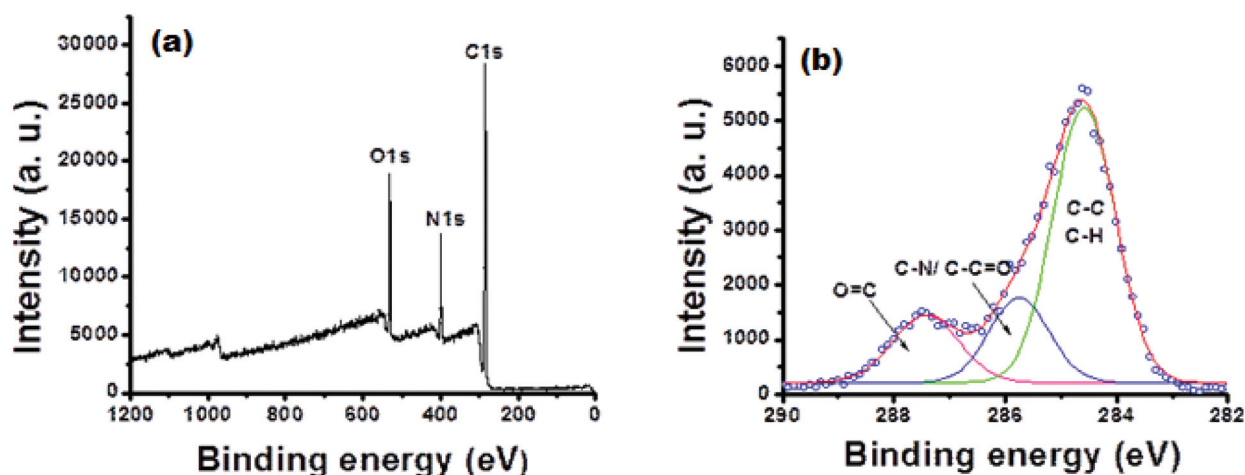|	NIPAM (g)	AA (µL)	BIS (mg)	KPS (mL)	Diameter (SEM)	Diameter (TEM)	Diameter (DLS)	Diameter (MRX)
A	0.2	10	20	0.2	890 nm	780 nm	1.0 µm	1.2 µm
B	0.3	15	30	0.3	1.15 µm	1.0 µm	1.4 µm	1.4 µm

Fig. 2 XPS spectra of the hydrogel@$SiO_2@Fe_3O_4$ particles: (a) a wide scan range and (b) a high-resolution spectrum of the C 1s peak that has been fitted with three component peaks, as further explained in the text.
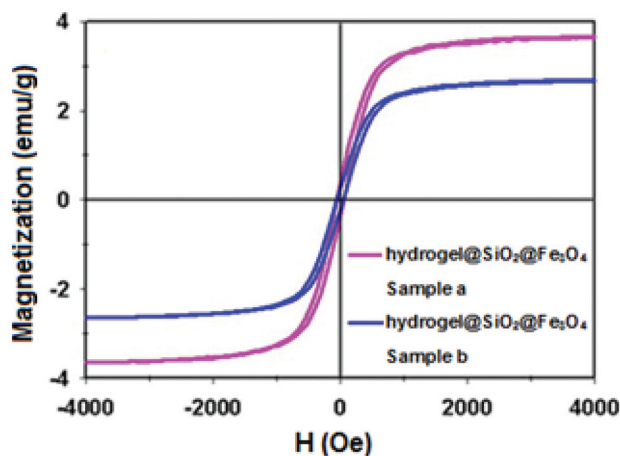
Fig. 3 Room temperature magnetic hysteresis curves of two distinct samples of hydrogel@SiO_2@Fe_3O_4 particles.

Fig. 4 UV-vis spectra of the Au_{rod} particles and the hybrid particles.

as compared to the Fe_3O_4 and SiO_2@Fe_3O_4 samples (hysteresis curves are provided in the ESI†), can be ascribed to the increase in non-magnetic layer components (silica and hydrogel).

Effect of external stimuli on the hybrid nanoparticles

Exposure of the hydrogel@SiO_2@Fe_3O_4 particles to various external stimuli (temperature, pH, NIR laser light, and oscillating magnetic fields) led to systematic and reversible variations in the hydrodynamic diameter (deswelling–swelling behavior) and therefore systematic and reversible variations in the optical absorbance/extinction of the hybrid particles. When a payload such as a drug, enzyme, or catalyst is loaded in the hydrogel, the shrinkage of the hydrogel can effect its release.[20] The stimuli-responsive volume changes in the hydrogel can thus be easily exploited in applications such as drug delivery. We report below the effect of each of these stimuli on the response of our hybrid nanoparticles.

The UV-vis spectra of the Au_{rod} particles and Au_{rods}@hydrogel@SiO_2@Fe_3O_4 hybrid particles are displayed in Fig. 4. The broad extinction bands for the hybrid particles resembles those of the Au_{rod} particles, where the transverse plasmon band appears at ~520 nm, and the longitudinal plasmon band appears at ~786 nm. The longitudinal band of the hybrid nanoparticles is slightly red-shifted (~11 nm) from those of the free Au_{rod} particles in aqueous solution due to the difference in the dielectric constant of the surrounding environment (80.4 for water and 2–4 for the hydrogel),[20,59] as well as the plasmon coupling of adjacent Au_{rods} in the hybrid particles.[19,20,22]

Thermally induced optical changes of the hybrid particles

To observe thermally induced changes to the particles, the temperature of the cuvette containing the dispersed particles was controlled using a temperature-controlled bath. As the particles reached a set temperature, we measured the UV-vis spectra and hydrodynamic radius using a UV-vis spectrometer
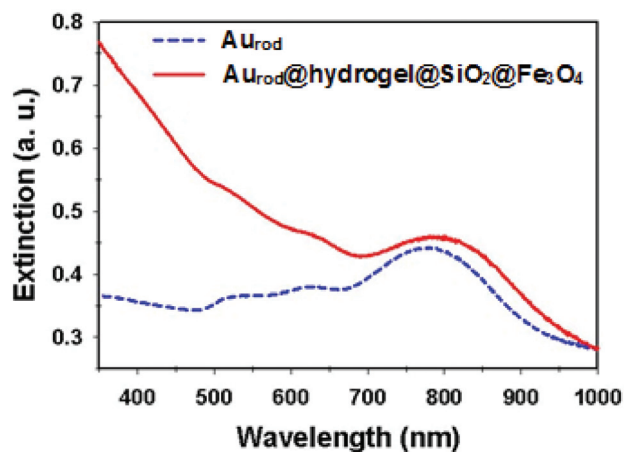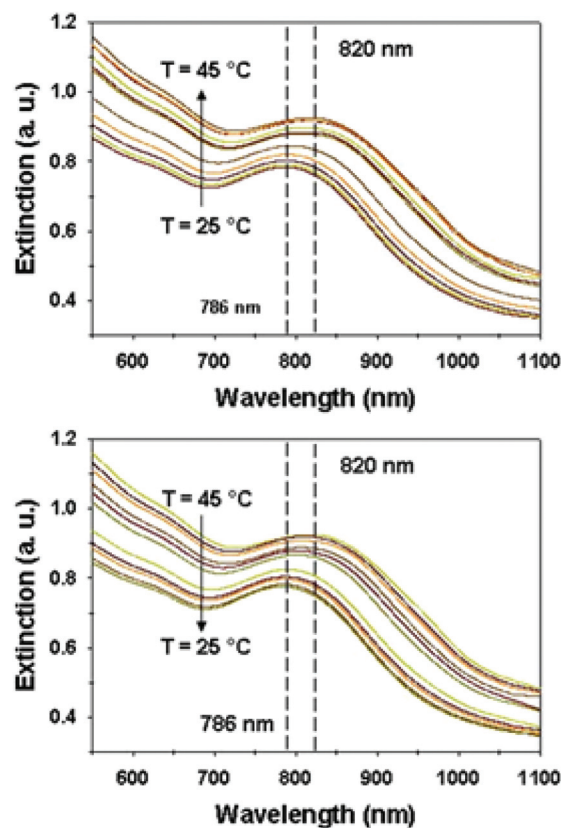

Fig. 5 Influence of temperature on the optical properties of the hybrid particles for a series of spectra collected at different temperatures (25–45 °C in 2 °C increments). Top: Increasing temperature; bottom: decreasing temperature. The dashed vertical lines indicate the longitudinal plasmon band at the starting and ending temperatures (786 nm and 820 nm at 25 °C and 45 °C, respectively).

and an ALV-5000 instrument, respectively. Fig. 5 shows the UV-vis spectra of the hybrid particles during various heating and cooling manipulations. Unlike the transverse plasmon band, the longitudinal plasmon band of the hybrid particles was sen-
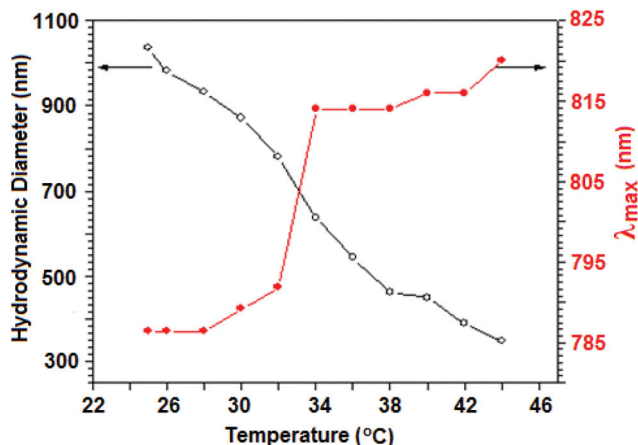
Fig. 6 Variation of the hydrodynamic diameter and the maximum of the longitudinal plasmon positions in the UV-visible spectra of the hybrid particles as a function of temperature.
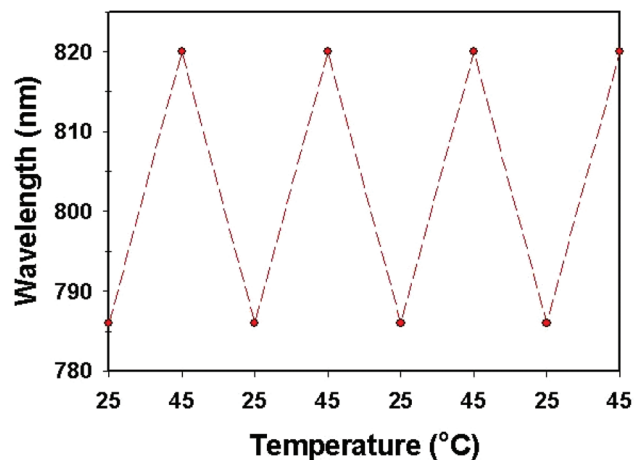

Fig. 7 Variation of λ_{max} as a function of cooling−heating events.

sitive to temperature. Consistent with previous studies,[19,20,22] the longitudinal band was observed to shift to a longer wavelength as the temperature increased due to a decrease in the distance between adjacent Au_{rod} particles upon contraction of the hydrogel layer. The relationship between the hydrodynamic diameter and the position of the longitudinal plasmon band of the hybrid particles as a function of temperature is plotted in Fig. 6.

At 25 °C, the hydrogel layer is in the swollen state, where the distance between adjacent Au_{rod} particles is relatively large, and the electronic interactions (plasmon coupling) between adjacent Au_{rod} particles is relatively weak. Conversely, at elevated temperatures, the hydrogel layer collapses, which decreases the distance between adjacent Au_{rod} particles and gives rise to strong coupling between adjacent Au_{rod} particles. Since the Au_{rod} particles are attached to the hydrogel layer in random orientations, various modes of coupling between adjacent Au_{rod} particles exist, but are predominantly end-to-end and end-to-side, which leads to the observed red shift, reduced absorption intensity, and broadening of the plasmon band.[19,20,22,62–65]

Additionally, the absorption intensity of the hybrid particle was observed to increase at elevated temperatures, which can be attributed to the contraction of the hydrogel layer and the consequent increase in the refractive index of that layer.[19,20,22] Notably, the sharpest change in red shift occurred between 33–35 °C, which is consistent with the lower critical solution temperature (LCST) of the hydrogel@SiO_2@Fe_3O_4 system as determined by DLS. The LCST is the temperature at which phase separation occurs and there is significant hydrogel shrinkage.[66] PNIPAM hydrogel possesses an LCST at ~32 °C and is known to undergo a large volume change at this temperature;[67] above the LCST, hydrogen bonding between water and the hydrophilic sites on the polymer backbone are disrupted and the hydrogen bonding network collapses.[68,69] This collapse leads to the formation of distinct domains with

different refractive indices, producing a change of as much as 10%.[70,71] For the collected data, the position and intensity of the plasmon bands were reproducible for several heating–cooling cycles (Fig. 7), which indicates that the hydrogel shell of the hybrid particles can undergo swelling–deswelling events reversibly without a detectable loss of Au_{rod} particles.

pH-Induced optical changes in the hybrid particles

We also explored the optical changes of the hybrid particles induced by changes in pH, using dilute solutions of hydrochloric acid and ammonium hydroxide to raise and lower the pH. With a pK_a of ~4, the carboxylic acid groups within the hydrogel layer are ionized over the pH range of 4–14, rendering the hydrogel with a net negative charge, which enables attachment of the positively charged Au_{rod} particles onto the negatively charged hydrogel *via* electrostatic interactions. In contrast, the electrostatic attraction decreases under highly acidic conditions (pH < 4), which can lead to the release of the Au_{rod} particles from the hydrogel.[22,25] Therefore, we investigated the optical changes of the hybrid particles over the pH range of 4–10. Fig. 8 shows the optical spectra of the hybrid particles recorded at rt for different pH values. At pH 4, the longitudinal plasmon band appeared at 800 nm, while at pH 7 and 10, it appeared at 786 nm. The shifting of the plasmon band can be explained in terms of a decrease in the distance between adjacent Au_{rod} particles upon contraction of the hydrogel layer. At pH 4, the distance between adjacent Au_{rod} particles was sufficiently short to allow interparticle interactions to occur because of the reduced surface area of the hydrogel; in contrast, at pH ≥ 7, the distance was greater because the same number of Au_{rod} particles were on a larger swollen hydrogel surface, which led to a reduction in the plasmon coupling. Notably, there was no change in the plasmon band positions at pH 7 and 10 because the hydrodynamic diameter of the hydrogel@SiO_2@Fe_3O_4 system was the same as determined by DLS (*i.e.*, ~1040 nm at both pH 7 and 10).
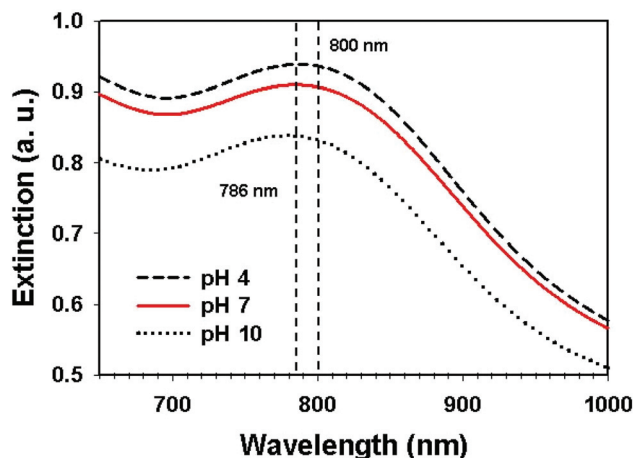
Fig. 8 Influence of pH on the optical properties of the hybrid particles.

Fig. 10 Change in temperature of (a) pure deionized water control experiment – blue line, (b) hydrogel@SiO$_2$@Fe$_3$O$_4$ particle suspension (composite particles without Au$_{rods}$) – dotted line, and (c) Au$_{rods}$@hydrogel@SiO$_2$@Fe$_3$O$_4$ particle suspension – red line, as a function of time upon irradiation at 808 nm at a power density of ∼5 W cm^{-2}.

Photo-induced optical changes in the hydrogel hybrid particles

Upon laser irradiation (AixiZ, CW 300 mW, 808 ± 10 nm), the longitudinal plasmon band of the hybrid particles shifted from 786 nm to 820 nm, as shown in Fig. 9. These results can be interpreted to indicate that the photothermal heating led to an increase in temperature near the Au$_{rod}$ particles and a collapsing of the hydrogel layer at the higher temperature, which gave rise to plasmonic coupling between adjacent Au$_{rod}$ particles. Furthermore, monitoring the temperature of the suspension during laser exposure revealed that the temperature of the hybrid particle suspension increased rapidly from ∼22 to 36 °C within 5 min, while the temperature in the control experiments (deionized water and hydrogel@SiO$_2$@Fe$_3$O$_4$ suspension) remained constant (see Fig. 10). These results confirm that the hybrid particles have the capacity to be heated photothermally in rapid fashion through plasmonic adsorption/scattering *via* the pendant Au$_{rod}$ particles.

Additionally, the hybrid particles were irradiated with the laser repeatedly, and the spectra were recorded after 15 min of
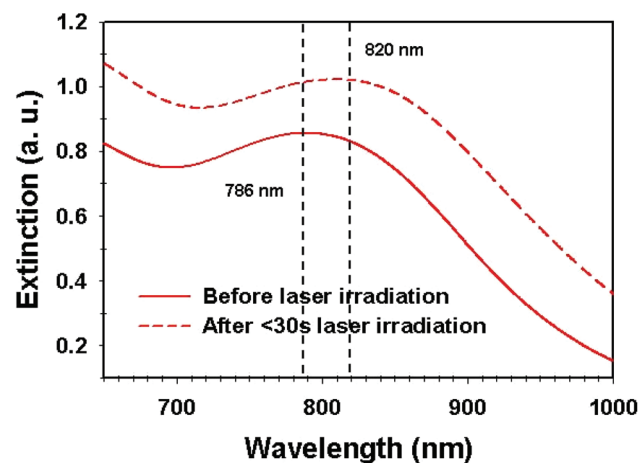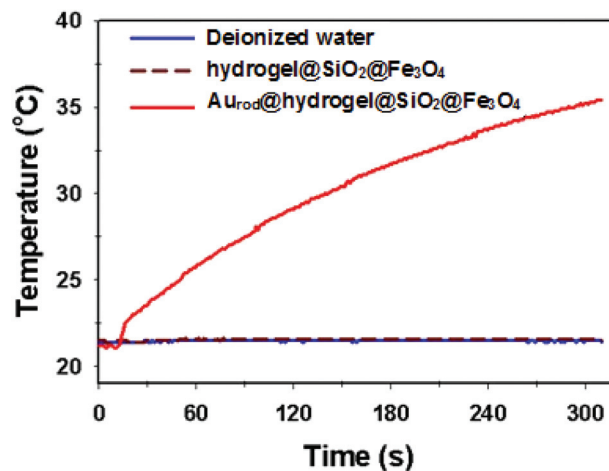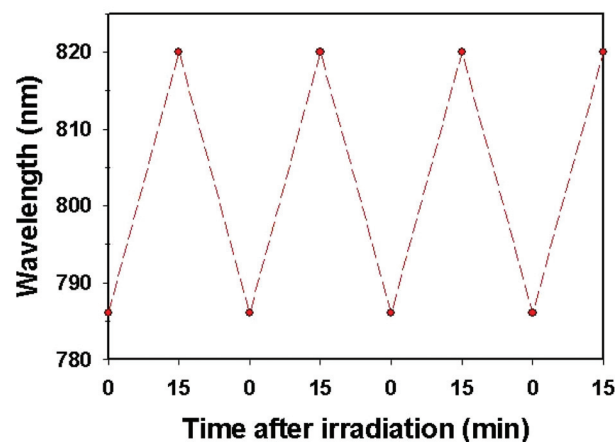

Fig. 11 Variation of λ_{max} as a function of time intervals after NIR laser irradiation.

laser irradiation and then after laser irradiation had been suspended for 15 min. Fig. 11 illustrates the position of the plasmon band as a function of time intervals during a series of laser irradiation exposures for the aqueous suspension containing the hybrid particles. Similar to the initial results observed for the thermally induced optical changes, the positions of the plasmon band alternate systematically during several cycles of laser irradiation, indicating again that no significant loss of the Au$_{rod}$ particles from the hybrid particle assembly occurs during the swelling–deswelling process.

Oscillating magnetic field-induced temperature changes in the hybrid particles

By applying an oscillating magnetic field, we anticipated a red-shifting of the plasmon band induced by the collapsing of the hydrogel layer due to the conduction of heat from the Fe$_3$O$_4$

Fig. 9 Influence of NIR laser irradiation on the optical properties of the hybrid particles.

core. The suspension of hybrid particles (concentration of Fe_3O_4 = 0.15 mg mL^{-1}) was exposed to an oscillating magnetic field of 10 kA m^{-1} at 100 kHz for 20 min. The absence of an increase in temperature implied that the hydrogel hybrid particles produced no measurable heat in the system, possibly due to the low concentration of Fe_3O_4 particles. Upon increasing the concentration of hybrid particles (concentration of Fe_3O_4 = 3 mg mL^{-1}), the temperature of the suspension of hybrid particles increased from 34 °C to a maximum temperature of ~40 °C within 10 min, and was maintained at this temperature more than 5 min as shown in Fig. 12. A slight increase in temperature (around 2 °C) after 10 min was also observed for the deionized water and the aqueous suspension of Au_{rods} samples due to direct heat transfer by conduction from the field coil.

On application of an alternating magnetic field, either the magnetic moments rotate or the nanoparticle itself rotates, and when the MNPs relax back to their original magnetic field orientation (Neel relaxation time, t_N, and Brownian relaxation time, t_B, respectively), heat is released. The generation of heat arises from the processes associated with these losses and the hysteresis losses.[72,73] In the case of large, ferromagnetic nanoparticles, such as those used in our experiment, heating occurs due to hysteresis losses and Brownian relaxation. Notably, the plot in Fig. 12 reveals that the temperature change in the suspension of Au_{rod} particles was similar to that of deionized water when exposed to an oscillating magnetic field, indicating that the Au_{rods} played no role in the production of heat energy for the hybrid particle system, and the additional 6 °C temperature increase can be attributed to the Fe_3O_4 MNP component. Although, our hybrid particles can produce sufficient heat energy to cause the hydrogel layer to collapse, inducing a red-shift in the plasmon band, the high concen-
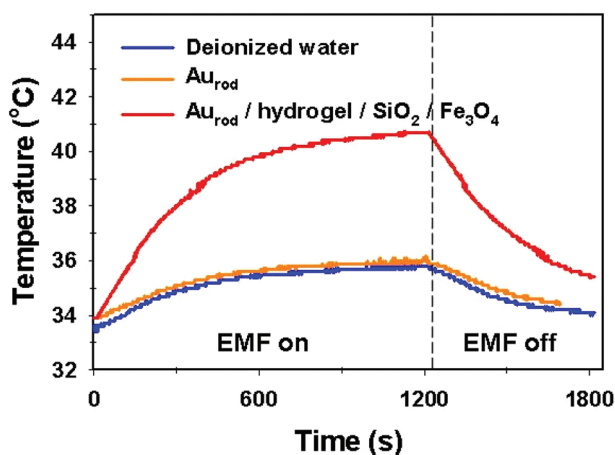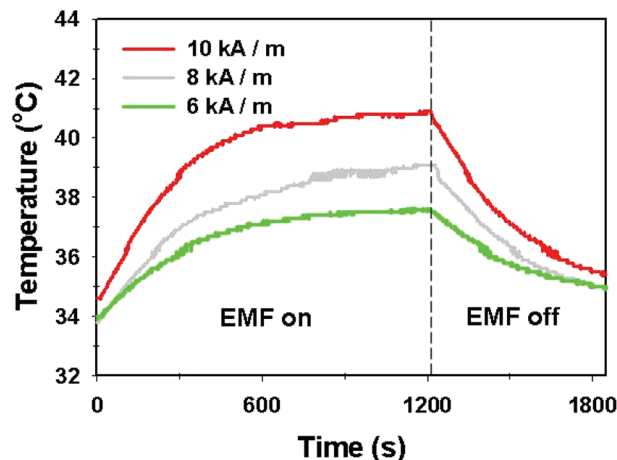

Fig. 13 Changes in temperature of aqueous suspensions of hybrid particles (3 mg mL^{-1} of Fe_3O_4) as a function of time under magnetic field strengths of 6, 8, and 10 kA m^{-1} at 100 kHz.

tration of hybrid particles necessary for this particular experiment, along with the high molar extinction of Au_{rod} particles,[74,75] adversely affected the absorption/extinction band, thereby inhibiting spectroscopic monitoring of the plasmon band.

The temperature increase arising from the hysteresis losses is proportional to the saturation magnetization of the MNPs.[76] We therefore studied the temperature changes induced by a variety of magnetic field strengths as a function of time. Predictably, higher maximum temperatures were obtained when higher magnetic field strengths were applied (see Fig. 13). At magnetic field strengths of 6 and 8 kA m^{-1}, the temperature increased from ~34 to 37 °C ($\Delta T \sim 3$ °C) and ~34 to 38 °C ($\Delta T \sim 4$ °C), respectively. In contrast, at a field strength of 10 kA m^{-1}, the temperature increased from ~34.5 °C to a maximum of ~40 °C ($\Delta T \sim 6$ °C) within 7 min and was maintained at the peak temperature for more than 10 min. The heating ability of the hybrid particles under oscillating magnetic fields, and the consequent triggering of the hydrogel layer to collapse, enables the realization of promising applications not only in a new paradigm of magnetically controlled drug release, but also in hyperthermia therapy.

Conclusions

Harnessing the unique properties of MNPs, Au_{rods}, and hydrogel coatings, we have successfully prepared silica-coated magnetic nanospheres encapsulated within thermo-responsive poly-(NIPAM-co-acrylic acid) hydrogels with Au_{rods} assembled on their surfaces. The hybrid particles were responsive to external stimuli, including temperature, pH, NIR light, and magnetic fields; the response was characterized by swelling–deswelling of the hydrogel volume with a consequent red-shifting of the plasmon band of the Au_{rods}. Due to the significant thermal and optical responses triggered by these external

Fig. 12 Change in temperature as a function of time under a magnetic field strength of 10 kA m^{-1} at 100 kHz for (a) deionized water, blue line – control experiment #1, (b) aqueous suspension of Au_{rod} particles, orange line – control experiment #2, and (c) aqueous suspension of the Au_{rods}@hydrogel@SiO$_2$@Fe$_3$O$_4$ hybrid particles (3 mg mL^{-1} of Fe_3O_4) – red line.

stimuli, our multi-responsive hybrid particles hold considerable promise for use in remotely-controlled drug delivery and hyperthermia therapy. Of course, for any specific application, only the most suitable and plausible stimulus will be chosen.

Conflict of Interest

The authors declare no competing financial interest.

Acknowledgements

References

1 S. Bhattacharya, F. Eckert, V. Boyko and A. Pich, *Small*, 2007, **3**, 650.

2 I. Berndt, J. S. Pedersen, P. Lindner and W. Richtering, *Langmuir*, 2006, **22**, 459.

3 R. H. Pelton and P. Chibante, *Colloids Surf.*, 1986, **20**, 247.

4 H. G. Schild, *Prog. Polym. Sci.*, 1992, **17**, 163.

5 C. D. Jones and L. A. Lyon, *Langmuir*, 2003, **19**, 4544.

6 G. Pasparakis and M. Vamvakaki, *Polym. Chem.*, 2011, **2**, 1234.

7 M. J. Snowden, B. Z. Chowdhry, B. Vincent and G. E. Morris, *J. Chem. Soc., Faraday Trans.*, 1996, **92**, 5013.

8 G. E. Morris, B. Vincent and M. J. Snowden, *J. Colloid Interface Sci.*, 1997, **190**, 198.

9 J. Guo, W. Yang, Y. Deng, C. Wang and S. Fu, *Small*, 2005, **1**, 737.

10 L. B. Chen, F. Zhang and C. C. Wang, *Small*, 2009, **5**, 621.

11 C. Liu, J. Guo, W. Yang, J. Hu, C. Wang and S. Fu, *J. Mater. Chem.*, 2009, **19**, 4764.

12 T.-Y. Liu, S.-H. Hu, K.-H. Liu, R.-S. Shaiu, D.-M. Liu and S.-Y. Chen, *Langmuir*, 2008, **24**, 13306.

13 C. M. Nolan, M. J. Serpe and L. A. Lyon, *Biomacromolecules*, 2004, **5**, 1940.

14 M. J. Serpe, K. A. Yarmey, C. M. Nolan and L. A. Lyon, *Biomacromolecules*, 2005, **6**, 408.

15 S. R. Sershen, S. L. Westcott, N. J. Halas and J. L. West, *J. Biomed. Mater. Res.*, 2000, **51**, 293.

16 J. Cai, J. Guo, M. Ji, W. Yang, C. Wang and S. Fu, *Colloid Polym. Sci.*, 2007, **285**, 1607.

17 J. Zhang, S. Xu and E. Kumacheva, *J. Am. Chem. Soc.*, 2004, **126**, 7908.

18 I. Gorelikov, L. M. Field and E. Kumacheva, *J. Am. Chem. Soc.*, 2004, **126**, 15938.

19 M. Karg, I. Pastoriza-Santos, J. Pérez-Juste, T. Hellweg and L. M. Liz-Marzán, *Small*, 2007, **3**, 1222.

20 M. Das, N. Sanson, D. Fava and E. Kumacheva, *Langmuir*, 2007, **23**, 196.

21 Y. Dong, Y. Ma, T. Zhai, F. Shen, Y. Zeng, H. Fu and J. Yao, *Macromol. Rapid Commun.*, 2007, **28**, 2339.

22 M. Karg, Y. Lu, E. Carbó-Argibay, I. Pastoriza-Santos, J. Pérez-Juste, L. M. Liz-Marzán and T. Hellweg, *Langmuir*, 2009, **25**, 3163.

23 C. C. Wang and F. Zhang, *Langmuir*, 2009, **25**, 8255.

24 T. Hoare, J. Santamaria, G. F. Goya, S. Irusta, D. Lin, S. Lau, R. Padera, R. Langer and D. S. Kohane, *Nano Lett.*, 2009, **9**, 3651.

25 M. Das, L. Mordoukhovski and E. Kumacheva, *Adv. Mater.*, 2008, **20**, 2371.

26 J. Zhang, K. Feng, M. Cuddihy, N. A. Kotov and P. X. Ma, *Soft Matter*, 2010, **6**, 610.

27 H. D. Hana, B. C. Shina and H. S. Choi, *Eur. J. Pharm. Biopharm.*, 2006, **62**, 110.

28 Y. Y. Liu, J. Lu and Y. H. Shao, *Macromol. Biosci.*, 2006, **6**, 452.

29 C. Wu and S. Zhou, *Macromolecules*, 1995, **28**, 8381.

30 C. Wu and S. Zhou, *Macromolecules*, 1996, **29**, 1574.

31 D. Gan and L. A. Lyon, *J. Am. Chem. Soc.*, 2001, **123**, 7511.

32 J. Wang, D. Gan, L. A. Lyon and M. A. El-Sayed, *J. Am. Chem. Soc.*, 2001, **123**, 11284.

33 J. D. Debord and L. A. Lyon, *Langmuir*, 2003, **19**, 7662.

34 S. Nayak and L. A. Lyon, *Chem. Mater.*, 2004, **16**, 2623.

35 S. Carregal-Romero, N. J. Buurma, J. Pérez-Juste, L. M. Liz-Marzán and P. Hervés, *Chem. Mater.*, 2010, **22**, 3051.

36 M. Zhou, F. Xing, M. Ren, Y. Feng, Y. Zhao, H. Qiu, X. Wang, C. Gao, F. Sun, Y. He, Z. Ma, P. Wen and J. Gao, *ChemPhysChem*, 2009, **10**, 523.

37 B. Luo, X. J. Song, F. Zhang, A. Xia, W. L. Yang, J. H. Hu and C. C. Wang, *Langmuir*, 2010, **26**, 1674.

38 R. Contreras-Cáceres, P. Pacifico, I. Pastoriza-Santos, J. Pérez-Juste, A. Fernández-Barbero and L. M. Liz-Marzán, *Adv. Funct. Mater.*, 2009, **19**, 3070.

39 T. Kawano, Y. Niidome, T. Mori, Y. Katayama and T. Niidome, *Bioconjugate Chem.*, 2009, **20**, 209.

40 S. Purushotham, P. E. J. Chang, H. Rumpel, I. H. C. Kee, R. T. H. Ng, P. K. H. Chow, C. K. Tan and R. V. Ramanujan, *Nanotechnology*, 2009, **20**, 305101.

41 T. M. Ruhland, P. M. Reichstein, A. P. Majewski, A. Walther and A. H. E. Mueller, *J. Colloid Interface Sci.*, 2012, **374**, 45.

42 Y. Deng, W. Yang, C. Wang and S. Fu, *Adv. Mater.*, 2003, **15**, 1729.

43 F. Zhang and C.-C. Wang, *Langmuir*, 2009, **25**, 8255.

44 J. Rubio-Retama, N. E. Zafeiropoulos, C. Serafinelli, O. Rojas-Reyna, B. Voit, E. L. Cabarcos and M. Stamm, *Langmuir*, 2007, **23**, 10280.

45 J. E. Wong, A. K. Gaharwar, D. Müller-Schulte, D. Bahadur and W. Richtering, *J. Colloid Interface Sci.*, 2008, **324**, 47.

46 F. Sauzedde, A. Elaõssari and C. Pichot, *Colloid Polym. Sci.*, 1999, **277**, 1041.

47 H. Chen, C. Deng and X. Zhang, *Angew. Chem., Int. Ed.*, 2009, **48**, 1.

48 L. Chen, H. Chen, X. Yao, X. Ma and H. Tian, *Chem. – Asian J.*, 2015, **10**, 2352.

49 B. Luo, X.-J. Song, F. Zhang, A. Xia, W.-L. Yang, J.-H. Hu and C.-C. Wang, *Langmuir*, 2010, **26**, 1674.

50 H. Deng, X. Li, Q. Peng, X. Wang, J. Chen and Y. Li, *Angew. Chem., Int. Ed.*, 2005, **44**, 2782.

51 W. Stöber, A. Fink and E. Bohn, *J. Colloid Interface Sci.*, 1968, **26**, 62.

52 J. H. Kim and T. R. Lee, *Chem. Mater.*, 2004, **16**, 3647.

53 E. M. Ahmed, *J. Adv. Res.*, 2015, **6**, 105.

54 B. Nikoobakht and M. A. El-Sayed, *Chem. Mater.*, 2003, **15**, 1957.

55 W. Stöber, A. Fink and E. Bohn, *J. Colloid Interface Sci.*, 1968, **26**, 62.

56 M. A. Correa-Duarte, M. Giersig, N. A. Kotov and L. M. Liz-Marzán, *Langmuir*, 1998, **14**, 6430.

57 Y. Lu, Y. Yin, B. T. Mayers and Y. Xia, *Nano Lett.*, 2002, **2**, 183.

58 A. P. Philipse, M. P. B. Van Bruggen and C. Pathmamanoharan, *Langmuir*, 1994, **10**, 92.

59 A. Gole and C. J. Murphy, *Chem. Mater.*, 2005, **17**, 1325.

60 M. A. Cole, N. H. Voelcker, H. Thissen and H. J. Griesser, *Biomaterials*, 2009, **30**, 1827.

61 L. K. Ista, S. Mendez, V. H. Perez-Luna and G. P. Lopez, *Langmuir*, 2001, **17**, 2552.

62 M. Gluodenis and C. A. Foss, *J. Phys. Chem. B*, 2002, **106**, 9484.

63 K. G. Thomas, S. Barazzouk, B. I. Ipe, S. T. S. Joseph and P. V. Kamat, *J. Phys. Chem. B*, 2004, **108**, 13066.

64 P. K. Sudeep, S. T. S. Joseph and K. G. Thomas, *J. Am. Chem. Soc.*, 2005, **127**, 6516.

65 M. A. Correa-Duarte, J. Pérez-Juste, A. Sánchez-Iglesias, M. Giersig and L. M. Liz-Marzán, *Angew. Chem., Int. Ed.*, 2005, **44**, 4375.

66 F.-Y. Chou, C.-M. Shih, M.-C. Tsai, W.-Y. Chiu and S. J. Lue, *Polymer*, 2012, **53**, 2839.

67 M. Prevot, C. Dejugnat, H. Mohwald and G. B. Sukhorukov, *ChemPhysChem*, 2006, **7**, 2497.

68 J.-H. Kim and T. R. Lee, *Drug Dev. Res.*, 2006, **67**, 61.

69 J.-K. Chen and C.-J. Chang, *Materials*, 2014, **7**, 805.

70 M. Kuang, D. Wang and H. Moehwald, *Adv. Funct. Mater.*, 2005, **15**, 1611.

71 B. W. Garner, Z. Hu, F. D. McDaniel and A. Neogi, *Mater. Res. Soc. Symp. Proc.*, 2008, 1060E.

72 R. Hergt, S. Dutz, R. Müller and M. Zeisberger, *J. Phys.: Condens. Matter*, 2006, **18**, S2919.

73 A. G. Kolhatkar, A. C. Jamison, D. Litvinov, R. C. Willson and T. R. Lee, *Int. J. Mol. Sci.*, 2013, **14**, 15977.

74 K. S. Lee and M. A. El-Sayed, *J. Phys. Chem. B*, 2005, **109**, 20331.

75 P. K. Jain, K. S. Lee, I. H. El-Sayed and M. A. El-Sayed, *J. Phys. Chem. B*, 2006, **110**, 7238.

76 J.-t. Jang, H. Nah, J.-H. Lee, S. H. Moon, M. G. Kim and J. Cheon, *Angew. Chem., Int. Ed.*, 2009, **48**, 1234.